mathematics

MDPI

Article

Low Dissipative Entropic Lattice Boltzmann Method

Oleg Ilyin

Federal Research Center "Computer Science and Control" of the Russian Academy of Sciences, Vavilova-44,2, 119333 Moscow, Russia; oilyin@gmail.com

Abstract: In the entropic lattice Boltzmann approach, the stability properties are governed by the parameter α, which in turn affects the viscosity of a flow. The variation of this parameter allows one to guarantee the fulfillment of the discrete H-theorem for all spatial nodes. In the ideal case, the alteration of α from its normal value in the conventional lattice Boltzmann method ($\alpha = 2$) should be as small as possible. In the present work, the problem of the evaluation of α securing the H-theorem and having an average value close to $\alpha = 2$ is addressed. The main idea is to approximate the H-function by a quadratic function on the parameter α around $\alpha = 2$. The entropy balance requirement leads to a closed form expression for α depending on the values of the H-function and its derivatives. To validate the proposed method, several benchmark problems are considered: the Sod shock tube, the propagation of shear, acoustic waves, and doubly shear layer. It is demonstrated that the obtained formula for α yields solutions that show very small excessive dissipation. The simulation results are also compared with the essentially entropic and Zhao–Yong lattice Boltzmann approaches.

Keywords: lattice Boltzmann; entropy; Padé approximations

MSC: 76P05; 76P99

Citation: Ilyin, O. Low Dissipative Entropic Lattice Boltzmann Method. *Mathematics* **2022**, *10*, 3928. https://doi.org/10.3390/math10213928

Academic Editor: Vasily Novozhilov

Received: 6 September 2022
Accepted: 19 October 2022
Published: 23 October 2022

1. Introduction

The lattice Boltzmann (LB) method has established itself as an alternative approach to the Navier–Stokes equations for the modeling of fluid motion. Due to its simplicity and high potential for parallel computing, the LB approach can be efficiently implemented in numerical solvers aimed at addressing academic and application-oriented problems [1–4]. Except for hydrodynamic problems, the LB approach has found applications in the modeling of porous media [5,6], microflows [7], multiphase, and other complex flows [8–11].

The standard realization of LB models is based on local collision and linear advection to adjacent lattice nodes in the direction of the corresponding discrete velocities. Such an approach is rather appealing due to its simplicity but is prone to instabilities when Mach (*Ma*) and Reynolds (*Re*) numbers are increased. Hence, additional stabilization techniques are usually adopted. These can be divided into several classes.

The instabilities usually manifest in oscillations, unphysical (negative) values of the hydrodynamic variables (density), and eventually in the breakdown of the solutions. It is possible to enhance the dissipative properties (and therefore stabilize the computations) of LB models by tuning the bulk viscosity [12]. This idea is generalized in the *multiple-relaxation-time* (MRT) LB method [13–15]. The drawback of this method is that acoustic waves show over-dissipative behavior due to the increased bulk viscosity. To maintain correct dissipation rates of acoustic waves, one can adopt selective viscosity filtering [16], which suppresses only high wave-number instabilities. In this approach, viscosity becomes dependent on the values of the wave-number. A simpler way of stabilizing the simulations is enforcement of the positivity of the solutions by adapting the relaxation time in the LB models [17]. This stabilization technique is rather straightforward but is less accurate than more sophisticated methods, such as the *entropic* LB (ELB) method [18]. In the ELB method, the stabilization is achieved by tuning the relaxation rates in order to satisfy the

H-theorem. The ELB approach requires two components [19,20]: the equilibrium state, which minimizes the H-function (entropy taken with minus sign), and the adjustable (in a special way) relaxation rate (the parameter α), which is evaluated from the significantly nonlinear entropy balance equation. Note that the standard equilibrium in the form of the polynomial function on the flow velocity is not suitable, since for this case the H-theorem is not valid [21,22]. The problem of construction of the entropic equilibrium states is non-trivial [23–26]. The solution α to the entropy balance equation can be obtained by applying the Newton–Raphson method, the bisection methods [27–29], or a combination of the Newton–Raphson method and analytical estimates [30]. In the essentially entropic approach, the solution to the entropy balance equation, which is reformulated as an inequality, has been obtained in an exact form by exploiting Padé approximations for the logarithms entering the entropy function [31]. This method yields solutions for α that have little deviation from its normal value ($\alpha = 2$). The entropic approach of Zhao and Yong relies on geometric considerations [32] (secant algorithm) and gives concise closed-form expressions for α. The comparison of several entropic methods has been performed recently [33]. Another class of entropic methods is based on the entropic limiters. In this approach, the non-equilibrium part of the distribution function is multiplied by a coefficient that depends on local non-equilibrium entropy [34–36]. This type of limiter has been successfully used for the modeling of supersonic flows with the LB method [37,38]. The entropic method can be extended for multiple relaxation time LB models. This approach uses decomposition of the distribution function into equilibrium, non-equilibrium hydrodynamic, and non-equilibrium non-hydrodynamic components. Non-equilibrium parts of the distribution function have different relaxation rates [39–42]. In order to satisfy the H-theorem, only the relaxation times for high-order moments are varied; hence, the viscosity remains unchanged.

In the *regularized* LB approach, the distribution function is projected onto some finite basis during each time step. The removal of the moments that cannot be described by the model leads to noticeable improvements in stability [43–45]. Furthermore, the concept of recursive regularization has been introduced, including thermal flows [46–52]. In the recursively regularized LB models, several non-equilibrium high-order moments are kept. Their values can be computed analytically as a special combination of low-order moments. In addition, variants of the regularized LB models in the relative reference frame have been proposed [53–55]. Note that the entropic LB and regularization methods share common features: regularized LB models maximize quadratic entropy [56]. In practice, however, the regularized LB models are usually more stable than un-regularized. Linear stability analysis shows that the regularization significantly changes the dissipation and dispersion properties of LB models [57–60]. Even more so, the regularized LB models can be unstable under some specific conditions for which un-regularized models are stable.

Another stabilization approach is focused on modification of the advection step. Employment of the standard streaming step means that the Courant number is equal to unity, and this can cause instabilities. Then, in order to reduce the Courant number, one can apply a *generalized* streaming step, for which the values of the distribution function in additional nodes are needed [61–65]. Numerical experiments indicate that the maximal stable Reynolds number for this method depends exponentially on the reduction of the Courant number. On the other hand, this method is more complicated than the standard one—for instance, the formulation of the boundary conditions requires additional efforts [66–68]

The aim of the present paper is to develop a variant of the entropic LB method in which the averaged deviations of the parameter α from its normal value, which equals 2, are minimized. This in turn means that the variations of the viscosity are also small and the dissipation properties of the modeled system are not distorted.

This paper is organized as follows. In Section 2, the main features of the entropic LB approach are considered. The formulation of the variational problem leading to the entropic equilibrium compatible with the hydrodynamic equations is performed by applying geometrical treatments; in addition, some pitfalls of the entropic method are discussed. In

Section 3, the derivation of a novel formula for α is presented. Since the entropy balance equation is a nonlinear transcendental equation, one cannot find an exact analytical solution α, but it is possible to obtain an approximate solution. This is performed in several steps. First, one finds an interval that contains the solution α; the lower (dissipative) bound and the upper bound of this interval are evaluated by applying Padé approximations for the logarithms. Then, the quadratic approximation of the H-function for α in the interval between the lower and upper bounds is constructed, and the entropy balance equation reduces to a quadratic algebraic equation for the variable α, which is solved analytically. In Section 4, the results of the numerical simulations are addressed: the shock tube problem, the propagation of shear and acoustic waves, and the doubly shear layer problem are solved by employing the essentially entropic, Zhao–Yong, and present method. In Section 5, the major results of the paper are outlined.

2. Entropic Lattice Boltzmann Method

In the present paragraph, the main ideas of the entropic lattice Boltzmann (ELB) approach are briefly recalled. The LB equation reads as follows [20]:

$$f_i(t + \Delta t, \boldsymbol{x} + \boldsymbol{c_i}\Delta t) = f_i(t, \boldsymbol{x}) + \alpha\beta(f_i^{eq} - f_i)(t, \boldsymbol{x}), \tag{1}$$

where f_i are the distribution functions corresponding to the particle velocities $\boldsymbol{c_i}$, $i = 1 \dots N$, f_i^{eq} are the local equilibrium distribution functions (their exact form is discussed below), $t, \boldsymbol{x}$ are time and spatial coordinates, and Δt is the time step. The variable $0 < \beta < 1$ is computed as

$$\beta = \frac{1}{2}\frac{\Delta t}{(\tau + \frac{1}{2}\Delta t)},$$

where τ is the relaxation time. In the standard LB method, the variable $\alpha = 2$ (α is also called the path length), τ is evaluated as $\nu = c_s^2\tau$, c_s is sound speed, and ν is viscosity. In the ELB method, the variable α is not constant and may change from node to node, and $\nu = (2/\alpha)c_s^2\tau$, while α is the solution of the following equation:

$$H[\boldsymbol{f} + \alpha(\boldsymbol{f^{eq}} - \boldsymbol{f})] \le H[\boldsymbol{f}], \tag{2}$$

where $H[\boldsymbol{f}]$ is a smooth convex function, $\boldsymbol{f} = \{f_i, i = 1 \dots N\}, and \boldsymbol{f^{eq}} = \{f_i^{eq}, i = 1 \dots N\}$. The form of the condition (2) is motivated by the following inequality:

$$H[\boldsymbol{f}(t + \Delta t, \boldsymbol{x} + \boldsymbol{c_i}\Delta t)] = H[\boldsymbol{f} + \alpha\beta(\boldsymbol{f^{eq}} - \boldsymbol{f})]$$

$$= H[(1 - \beta)\boldsymbol{f} + \beta(\boldsymbol{f} + \alpha(\boldsymbol{f^{eq}} - \boldsymbol{f}))] \le (1 - \beta)H[\boldsymbol{f}] + \beta H[\boldsymbol{f} + \alpha(\boldsymbol{f^{eq}} - \boldsymbol{f})]$$

$$\le (1 - \beta)H[\boldsymbol{f}] + \beta H[\boldsymbol{f}] = H[\boldsymbol{f}],$$

where the convexity property for the function H was used, and the condition (2) was applied. Hence, the condition (2) guarantees the fulfillment of the H-theorem, and the entropy is increased by the collisions (the H-function is decreasing). Note that the explicit form of the function $H[f]$ is not needed in the derivation of the H-theorem. The usual form of the H-function in the LB theory is Boltzmann-like, that is,

$$H[\boldsymbol{f}] = \sum_i f_i \log\left(\frac{f_i}{w_i}\right),$$

where $w_i > 0$ are the lattice weights (discrete analogs of the absolute Maxwell distribution).

One should emphasize that the ELB approach is based on two components: the equilibrium f_i^{eq} (entropic equilibrium), which is a minimum of the H function, and a parameter α, which is tuned in order to guarantee a discrete H-theorem. The presence of both components is crucial. The entropic equilibrium is a non-polynomial function of the

flow velocity. For the one-dimensional three-velocity model ($D1Q3$), the following entropic equilibrium can be used [69]:

$$f_{\pm 1} = \frac{1}{3}\rho\left(\pm\frac{uc \mp c_s^2}{2c_s^2} + \sqrt{1+\frac{u^2}{c_s^2}}\right), \tag{3}$$

$$f_0 = \frac{2}{3}\rho\left(2 - \sqrt{1+\frac{u^2}{c_s^2}}\right), \tag{4}$$

where $f_{\pm 1}, f_0$ correspond to the particles with the velocities $\pm c, 0$; ρ, u are the density and the flow velocity; and $c_s = c/\sqrt{3} = 1/\sqrt{3}$, since in the present study $c = 1$. The extension of the equilibrium (3)–(4) for the two-dimensional nine-velocity model ($D2Q9$) is based on the product of two equilibrium functions for the $D1Q3$ model.

The variation of the path length variable α controls the dissipation properties of the flow via increase or decrease of the viscosity. Equation (2) can have solutions $\alpha < 2$; this means that the stabilization is needed and the viscosity of the flow is increased. In the case $\alpha > 2$, the viscosity is decreased. In the perfect case, the alteration of α from 2 should be as small as possible since this guarantees that the distortion of the viscosity of the modeled flow is minimal.

Following the previous studies, it would be convenient to introduce a scalar product as follows:

$$(\boldsymbol{a}, \boldsymbol{b}) = \sum_i^N a_i b_i,$$

where $\boldsymbol{a}, \boldsymbol{b}$ are two vectors with the components $a_i, b_i, i = 1 \ldots N$. Then, the macroscopic variables—density ρ, momentum $\rho\boldsymbol{u}$—can be computed as

$$(\boldsymbol{f}, 1) = \rho, \quad (\boldsymbol{f}, \boldsymbol{c}_\gamma) = \rho \boldsymbol{u}_\gamma,$$

where γ denotes the spatial coordinates x, y, z.

Note that in terms of the introduced scalar products, the H-function can rewritten as follows:

$$H[\boldsymbol{f}] = (\boldsymbol{f}, \log(\boldsymbol{f}/\boldsymbol{w})).$$

where $\boldsymbol{w} = \{w_i, i = 1 \ldots N\}$.

The formulation of the problem for finding f_i^{eq} has some subtleties. It would be instructive to consider this problem in detail. For athermal flows, the hydrodynamic fields ρ and $\boldsymbol{u}$ are conserved during the collisions, but the energy $\rho c_s^2 + \rho u^2 = \sum_i f_i c_i^2$ is not a collision invariant. Then, $D+1$ quantities remain unchanged due to collisions, where D is the number of spatial dimensions. For a given ρ and $\boldsymbol{u}$, the discrete distribution functions $f_i, i = 1 \ldots N$ define a manifold denoted by S in $\mathbb{R}^N$, an the dimension of S equals $N - (D+1)$. The entropic local equilibrium state f_i^{eq} is then a point in S for which a minimum of $H[\boldsymbol{f}]$ is attained. One has the following:

$$\begin{cases} \boldsymbol{f}^{eq} : \min_{f_i, i=1\ldots N} H[\boldsymbol{f}] \\ G_1(\boldsymbol{f}) = G_2(\boldsymbol{f}) = \ldots = G_{D+1}(\boldsymbol{f}) = 0 \end{cases} \tag{5}$$

where $G_j = 0, j = 1 \ldots D+1$ denote the constraints $\sum_i f_i - \rho = 0, \sum_i f_i c_{i,\gamma} - \rho u_\gamma = 0$. It is important to mention that it is not correct to replace $\boldsymbol{f}$ by $\boldsymbol{f}^{eq}$ in the constraints in Equation (5).

The geometrical interpretation of the problem is presented in Figure 1. Consider a point $\boldsymbol{f}$ in S, and let $\boldsymbol{f}(\epsilon)$ be a curve in S parameterized by $\epsilon \geq 0$ such that $\boldsymbol{f}(0) = \boldsymbol{f}$. By applying the Taylor expansion one obtains the following:

$$\boldsymbol{f}(\epsilon) = \boldsymbol{f} + \epsilon \boldsymbol{\delta f} + o(\epsilon),$$

where $\delta \boldsymbol{f}$ is a vector in the tangent space defined as $T_f(S)$ to the manifold S at the point $\boldsymbol{f}$. Now, assume that $\boldsymbol{f}$ is a minimum of $H[\boldsymbol{f}]$; then,

$$\frac{dH[\boldsymbol{f}(\epsilon)]}{d\epsilon}|_{\epsilon=0} = 0,$$

On the other hand,

$$\frac{dH[\boldsymbol{f}(\epsilon)]}{d\epsilon}|_{\epsilon=0} = \frac{dH[\boldsymbol{f} + \epsilon\delta\boldsymbol{f} + o(\epsilon)]}{d\epsilon}|_{\epsilon=0} = (\boldsymbol{\nabla} H[\boldsymbol{f}], \delta\boldsymbol{f}),$$

where $\boldsymbol{\nabla} H[\boldsymbol{f}] = dH[\boldsymbol{f}]/d\boldsymbol{f}$. Finally, one gets

$$(\boldsymbol{\nabla} H[\boldsymbol{f}], \delta\boldsymbol{f}) = 0,$$

Hence, $\boldsymbol{\nabla} H[\boldsymbol{f}]$ belongs to an orthogonal complement to the tangent space $T_f(S)$, which is defined as $T_f(S)^\perp$, and obviously $T_f(S) \oplus T_f(S)^\perp = \mathbb{R}^N$. Remember that the manifold S is specified by the conditions $G_j = 0, j = 1 \ldots N$; then, $\boldsymbol{\nabla} G_j$ are normal vectors to S, and they can be considered as a basis in $T_f(S)^\perp$. Therefore,

$$\boldsymbol{\nabla} H[\boldsymbol{f}] = \sum_{j=1}^{D+1} \lambda_j \boldsymbol{\nabla} G_j, \tag{6}$$

where λ_j are expansion coefficients, which can be recognized as Lagrange multipliers.

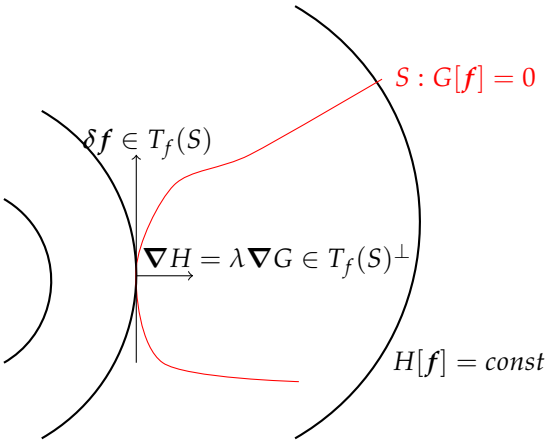

Figure 1. Contour lines of the function $H[f]$, the constraints surface $S : G[\boldsymbol{f}] = 0$, the elements of the tangent spaces $T_f(S)$, and the complement to the tangent space $T_f(S)^\perp$ are presented.

Equation (6) is solved jointly with the constraints $G_j = 0$. Not all equilibrium states are allowed from the physical point of view. Obviously, the considered model should lead to correct hydrodynamics. In order to recover Navier–Stokes equations (at least with $O(u^3)$ error), it is sufficient to include the following additional condition [70]:

$$\sum_i f_i^{eq} c_{i,\gamma} c_{i,\kappa} = \rho u_\gamma u_\kappa + \rho c_s^2 \delta_{\gamma\kappa}. \tag{7}$$

It is worth emphasizing that one cannot replace $\boldsymbol{f}^{eq}$ by $\boldsymbol{f}$ in Equation (7), since the condition (7) holds only for the equilibrium part of the distribution function. The equilibrium distribution function, which also respects the condition (7), is termed *perfect*.

The form of the solution for the problem (5), (7) depends on the particular choice of $H[\boldsymbol{f}]$. As has been mentioned before, the Boltzmann $H[\boldsymbol{f}]$ is the most popular vari-

ant. However, one may consider a simpler variant—quadratic entropy, which takes the following form:

$$H[f] = \sum_i \frac{f_i^2}{w_i},$$

This function plays a role in the regularization of LB models, namely, regularized LB models minimize the quadratic H-function [56]. It is tempting to apply quadratic entropy in the ELB approach. Firstly, consider the Equation (2) in the form of equality. The solution is as follows [69]:

$$\alpha = -\frac{2\sum_i \frac{(f_i^{eq}-f_i)f_i}{w_i}}{\sum_i \frac{(f_i^{eq}-f_i)^2}{w_i}},$$

Hence, one has a closed-form expression for α that exactly solves the entropy balance equation. Next, one needs to find the equilibrium states from the problem (5). From (5) and (6), one gets the following:

$$f_i^{eq} = \rho w_i \left(1 + \frac{\boldsymbol{c_i u}}{c_s^2}\right),$$

The obtained equilibrium depends linearly on the flow velocity $\boldsymbol{u}$; hence, it cannot be perfect. In addition, as was mentioned in the previous studies [69], this equilibrium admits negative values, and this can lead to negative density. As a final remark, it can be argued that some caution is necessary in the selection of the H-function and the local equilibrium in the ELB method. In the present study, the equilibrium (3)–(4) is used, which is entropic (minimizes Boltzmann H-function) and perfect.

3. Low-Dissipative ELB Method

For the Boltzmann entropy, the Equation (2)

$$H[\boldsymbol{f} + \alpha(\boldsymbol{f^{eq}} - \boldsymbol{f})] \le H[\boldsymbol{f}]$$

is rewritten as [31,71]

$$(\boldsymbol{f}, (1+\alpha\boldsymbol{x})\log(1+\alpha\boldsymbol{x})) \le \alpha(\boldsymbol{f}, \boldsymbol{x}\log(1+\boldsymbol{x})), \tag{8}$$

where the variable $\boldsymbol{x}$ measures the departure from the local equilibrium

$$\boldsymbol{x} = \frac{\boldsymbol{f^{eq}} - \boldsymbol{f}}{\boldsymbol{f}}$$

and has the components $x_i = (f_i^{eq} - f_i)/f_i$. It would be convenient to introduce the following scalar products:

$$(a,b)_+ = \sum_{i:x_i \ge 0} a_i b_i, \quad (a,b)_- = \sum_{i:x_i < 0} a_i b_i,$$

where $\boldsymbol{a}, \boldsymbol{b}$ are two vectors with the components $a_i, b_i, i = 1 \ldots N$. The general idea for solving Equation (2) or (8) is as follows. At the first step, the bounds for the minimal values of α denoted as $\underline{\alpha}$ ($\underline{\alpha} \le 2$) are evaluated from (8). At the second step, the upper bounds for α denoted as $\overline{\alpha}$ ($\overline{\alpha} \ge 2$) are computed. Next, the function $H[\boldsymbol{f} + \alpha(\boldsymbol{f^{eq}} - \boldsymbol{f})]$ is approximated by a quadratic function of the variable $\alpha - 2$ in the interval $[\underline{\alpha}, 2]$, and a similar approximation is performed in the interval $[2, \overline{\alpha}]$. Finally, the estimates for $\alpha \in [\underline{\alpha}, \overline{\alpha}]$ (termed low-dissipative) are evaluated by solving a quadratic equation. The geometric interpretation of the proposed method is presented in Figure 2.

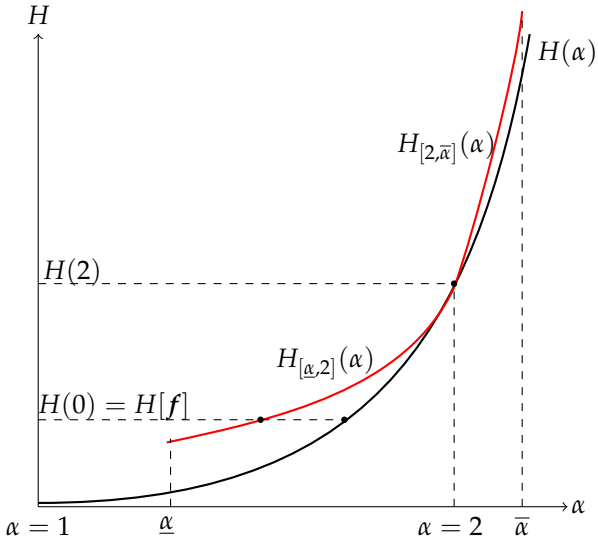

Figure 2. The geometric interpretation of the present method; $H(\alpha) \equiv H[\boldsymbol{f} + \alpha(\boldsymbol{f}^{eq} - \boldsymbol{f})]$ and $H_{[\underline{\alpha},2]}(\alpha), H_{[2,\overline{\alpha}]}(\alpha)$ are quadratic approximations of $H(\alpha)$ in the intervals $[\underline{\alpha}, 2]$ and $[2, \overline{\alpha}]$.

3.1. Bounds for the Logarithm

To obtain the values of $\underline{\alpha}, \overline{\alpha}$, one needs to find lower and upper bounds of the logarithm. The most natural way of doing this is to apply the Padé approximations, which are based on rational functions. Such an approach has been used in the essentially entropic LB method [31,71]. Following Topsøe [72], one has a chain of inequalities for $z > 0$ as follows:

$$\phi_1(z) \le \phi_2(z) \le \ldots \le \log(1+z) \le \ldots \le \psi_2(z) \le \psi_1(z), \tag{9}$$

where the first lower approximants $\phi_n(z)$ in (9) are given by

$$\phi_1(z) = \frac{2z}{2+z}, \quad \phi_2(z) = \frac{3z(2+z)}{6+6z+z^2},$$

and the first upper approximants $\psi_n(z)$ are

$$\psi_1(z) = \frac{z(2+z)}{2(1+z)}, \quad \psi_2(z) = \frac{z(6+z)}{2(3+2z)}.$$

In order to derive the bounds for $z \in (-1, 0]$, the duality between functions in the intervals $z \in (-1, 0]$ and $z \in [0, \infty)$ is introduced. For the function $g(z)$, the dual function $g^*(z)$ is defined by the rule

$$g^*(z) = -g\left(-\frac{z}{1+z}\right),$$

It is obvious that $z \to -\frac{z}{1+z}$ maps $[0, \infty)$ onto $(-1, 0]$. Note that the dual function for $\log(1+z)$ is $\log(1+z)$ (i.e., this function is self-dual). Therefore, the following inequalities are obtained for $-1 < z \le 0$ by applying the duality properties to (9)

$$\psi_1^*(z) \le \psi_2^*(z) \le \ldots \le \log(1+z) \le \ldots \le \phi_2^*(z) \le \phi_1^*(z). \tag{10}$$

In addition, the following inequality is valid for any $z > -1$:

$$\phi_0(z) \le \log(1+z) \le \psi_0(z), \tag{11}$$

where

$$\phi_0(z) = \frac{z}{1+z}, \quad \psi_0(z) = z.$$

In the present study, it would be convenient to apply the following upper bound for $z \in (-1, 0]$ instead of $\log(1+z) \leq \phi_n^*(z)$:

$$\log(1+z) \leq \sum_{l=1}^{M} (-1)^{(l+1)} \frac{z^l}{l}. \tag{12}$$

3.2. Evaluation of $\underline{\alpha}$

The value of $\underline{\alpha}$ is obtained as a particular solution of (8). For the present method, it serves as a lower bound. Note that $\underline{\alpha}$ can be used as a stabilizer for LB models, but in practice, it leads to dissipative behavior.

Consider the Equation (8). Since α is not inside the logarithmic function in the right hand side of (8), approximation of only the left-hand side is needed. Assume that one finds a function $A(\alpha)$ such that

$$(\boldsymbol{f}, (1+\alpha \boldsymbol{x}) \log(1+\alpha \boldsymbol{x})) \leq A(\alpha) \leq \alpha(\boldsymbol{f}, \boldsymbol{x} \log(1+\boldsymbol{x}))$$

for $\alpha \geq 1$; then, the fulfillment of $A(\alpha) \leq \alpha(\boldsymbol{f}, \boldsymbol{x} \log(1+\boldsymbol{x}))$ means that the inequality (8) is satisfied.

One has

$$(\boldsymbol{f}, (1+\alpha \boldsymbol{x}) \log(1+\alpha \boldsymbol{x})) = (\boldsymbol{f}, (1+\alpha \boldsymbol{x}) \log(1+\alpha \boldsymbol{x}))_+ + (\boldsymbol{f}, (1+\alpha \boldsymbol{x}) \log(1+\alpha \boldsymbol{x}))_-,$$

where the first term in this sum is approximated with use of the inequality from (9).

$$(\boldsymbol{f}, (1+\alpha \boldsymbol{x}) \log(1+\alpha \boldsymbol{x}))_+ \leq (\boldsymbol{f}, (1+\alpha \boldsymbol{x}) \psi_1(\alpha \boldsymbol{x}))_+ = (\boldsymbol{f}, \frac{1}{2} \alpha \boldsymbol{x}(2+\alpha \boldsymbol{x}))_+, \tag{13}$$

For the second term, the inequality (12) for $M = 3$ is applied.

$$(\boldsymbol{f}, (1+\alpha \boldsymbol{x}) \log(1+\alpha \boldsymbol{x}))_- \leq (\boldsymbol{f}, (1+\alpha \boldsymbol{x})(\alpha \boldsymbol{x} - \frac{1}{2}(\alpha \boldsymbol{x})^2 + \frac{1}{3}(\alpha \boldsymbol{x})^3))_-, \tag{14}$$

Hence, $A(\alpha)$ is a sum of (13) and (14). Using $(\boldsymbol{f}, \boldsymbol{x}) = 0$, the inequality $A(\alpha) \leq \alpha(\boldsymbol{f}, \boldsymbol{x} \log(1+\boldsymbol{x}))$ is rewritten as

$$\frac{\alpha}{2}(\boldsymbol{f}, \boldsymbol{x}^2) - \frac{\alpha^2}{6}(\boldsymbol{f}, \boldsymbol{x}^3)_- + \frac{\alpha^3}{3}(\boldsymbol{f}, \boldsymbol{x}^4)_- \leq (\boldsymbol{f}, \boldsymbol{x} \log(1+\boldsymbol{x})). \tag{15}$$

Now, one can prove the following:

Lemma 1. *If α satisfies (15), then $\alpha \leq 2$.*

Proof. Note that from (11), it follows that $(\boldsymbol{f}, \boldsymbol{x} \log(1+\boldsymbol{x})) \leq (\boldsymbol{f}, \boldsymbol{x}^2)$. In addition, since $\alpha \geq 1$, $\frac{1}{2}(\boldsymbol{f}, \boldsymbol{x}^2) - \frac{\alpha}{6}(\boldsymbol{f}, \boldsymbol{x}^3)_- + \frac{\alpha^2}{3}(\boldsymbol{f}, \boldsymbol{x}^4)_- \geq \frac{1}{2}(\boldsymbol{f}, \boldsymbol{x}^2) - \frac{1}{6}(\boldsymbol{f}, \boldsymbol{x}^3)_- + \frac{1}{3}(\boldsymbol{f}, \boldsymbol{x}^4)_- \geq 0$. One has

$$\alpha \leq \frac{(\boldsymbol{f}, \boldsymbol{x} \log(1+\boldsymbol{x}))}{\frac{1}{2}(\boldsymbol{f}, \boldsymbol{x}^2) - \frac{\alpha}{6}(\boldsymbol{f}, \boldsymbol{x}^3)_- + \frac{\alpha^2}{3}(\boldsymbol{f}, \boldsymbol{x}^4)_-} \leq \frac{(\boldsymbol{f}, \boldsymbol{x}^2)}{\frac{1}{2}(\boldsymbol{f}, \boldsymbol{x}^2) - \frac{1}{6}(\boldsymbol{f}, \boldsymbol{x}^3)_- + \frac{1}{3}(\boldsymbol{f}, \boldsymbol{x}^4)_-} \leq 2.$$

□

Applying Lemma 1, one has for the left-hand side of (15)

$$\frac{\alpha}{2}(\boldsymbol{f}, \boldsymbol{x}^2) - \frac{\alpha^2}{6}(\boldsymbol{f}, \boldsymbol{x}^3)_- + \frac{\alpha^3}{3}(\boldsymbol{f}, \boldsymbol{x}^4)_- \leq \alpha \left(\frac{1}{2}(\boldsymbol{f}, \boldsymbol{x}^2) - \frac{1}{3}(\boldsymbol{f}, \boldsymbol{x}^3)_- + \frac{4}{3}(\boldsymbol{f}, \boldsymbol{x}^4)_- \right)$$

Finally, redefining the function $A(\alpha)$ as $\alpha \left(\frac{1}{2}(\boldsymbol{f}, \boldsymbol{x}^2) - \frac{1}{3}(\boldsymbol{f}, \boldsymbol{x}^3)_- + \frac{4}{3}(\boldsymbol{f}, \boldsymbol{x}^4)_- \right)$, one finds the value of $\underline{\alpha}$ as

$$\underline{\alpha} = \frac{(\boldsymbol{f}, \boldsymbol{x}\log(1+\boldsymbol{x}))}{\left(\frac{1}{2}(\boldsymbol{f}, \boldsymbol{x}^2) - \frac{1}{3}(\boldsymbol{f}, \boldsymbol{x}^3)_- + \frac{4}{3}(\boldsymbol{f}, \boldsymbol{x}^4)_-\right)}. \tag{16}$$

As a remark, one can notice that it is possible to take $M > 3$ in the inequality (12) applied in (14), but the numerical simulations show that the difference will be relatively small in comparison to Equation (16).

3.3. Evaluation of $\overline{\alpha}$

From the condition $f_i + \alpha(f_i^{eq} - f_i) \geq 0, i = 1 \ldots N$, one obtains the upper bound α^* [28] for the variable α as follows:

$$\alpha \leq \alpha^* = \min_{i: f_i - f_i^{eq} > 0} \frac{f_i}{f_i - f_i^{eq}}, \tag{17}$$

In the present paragraph, an additional upper bound defined as $\overline{\alpha}$ is evaluated. Assume that one finds a function $B(\alpha)$ such that

$$B(\alpha) \leq (\boldsymbol{f}, (1+\alpha\boldsymbol{x})\log(1+\alpha\boldsymbol{x})) \leq \alpha(\boldsymbol{f}, \boldsymbol{x}\log(1+\boldsymbol{x}))$$

for all $\alpha \geq 1$. Then, the solution to the equation $B(\alpha) = \alpha(\boldsymbol{f}, \boldsymbol{x}\log(1+\boldsymbol{x}))$ defines the upper bound. One has

$$(\boldsymbol{f}, (1+\alpha\boldsymbol{x})\log(1+\alpha\boldsymbol{x})) \geq (\boldsymbol{f}, (1+\alpha\boldsymbol{x})\phi_0(\alpha\boldsymbol{x}))_+$$

$$+(\boldsymbol{f}, (1+\alpha\boldsymbol{x})\psi_1^*(\alpha\boldsymbol{x}))_- = \frac{\alpha^2}{2}(\boldsymbol{f}, \boldsymbol{x}^2)_- \equiv B(\alpha),$$

Note that $\psi_1^* = \psi_1$ has been used. Then,

$$\overline{\alpha} = \frac{2(\boldsymbol{f}, \boldsymbol{x}\log(1+\boldsymbol{x}))}{(\boldsymbol{f}, \boldsymbol{x}^2)_-} \geq 2. \tag{18}$$

3.4. Explicit Formula for α

In this paragraph, the quadratic on α functions, which serve as an upper bound for $H(\alpha)$ in the interval $[\underline{\alpha}, \overline{\alpha}]$, where $H(\alpha) = H[\boldsymbol{f} + \alpha(\boldsymbol{f}^{eq} - \boldsymbol{f})]$, are constructed (Figure 2).

First, assume that the flow is far from equilibrium and α^*, defined by Equation (17), is smaller than 2. In this case, as a solution of (8), the value $\alpha = \min(\underline{\alpha}, \alpha^*)$, where $\underline{\alpha}$, defined by (16), is taken. In practice, this is a very rare event.

Consider the case $\alpha^* > 2$ and $H[\boldsymbol{f}] = H(0) \leq H(2)$, then the solution α of Equation (8) belongs to the interval $[\underline{\alpha}, 2]$. Consider the Taylor expansion of the function $H(\alpha)$ at $\alpha = 2$ with the residual in the form of Lagrange, as follows:

$$H(\alpha) = H(2) + H_\alpha(2)(\alpha - 2) + \frac{1}{2!}H_{\alpha\alpha}(\theta)(\alpha - 2)^2,$$

where $\alpha \in [\underline{\alpha}, 2]$. Then, θ is in the interval $[\underline{\alpha}, 2]$. Note that

$$H_\alpha(\alpha) = (\boldsymbol{f}, \boldsymbol{x}\log(1+\alpha\boldsymbol{x})) - (\boldsymbol{f}, \boldsymbol{x}\log(1+x)),$$

$$H_{\alpha\alpha}(\alpha) = \left(\boldsymbol{f}, \frac{\boldsymbol{x}^2}{1+\alpha\boldsymbol{x}}\right),$$

Let us construct the function $H_{[\underline{\alpha},2]}(\alpha) \geq H(\alpha), \alpha \in [\underline{\alpha}, 2]$ as

$$H_{[\underline{\alpha},2]}(\alpha) = H(2) + H_\alpha(2)(\alpha - 2) + \frac{1}{2!}\overline{H}_{[\underline{\alpha},2]}(\alpha - 2)^2, \tag{19}$$

where

$$H_{\alpha\alpha}(\theta) \leq \max_{\alpha\in[\underline{\alpha},2]} H_{\alpha\alpha}(\theta)$$

$$\leq \left(f, \frac{x^2}{1+\underline{\alpha}x}\right)_+ + \left(f, \frac{x^2}{1+2x}\right)_- \equiv \overline{H}_{[\underline{\alpha},2]}. \tag{20}$$

Next, consider the case $\alpha^* > 2$ and $H[f] = H(0) \geq H(2)$; then, $\alpha \in [2, \min(\overline{\alpha}, \alpha^*)]$. If $\alpha^* \leq \overline{\alpha}$, then $\alpha = 2$ is adopted as a solution of Equation (8). If $\alpha^* > \overline{\alpha}$, then, similarly to the previous case, the function $H_{[2,\overline{\alpha}]}(\alpha) \geq H(\alpha), \alpha \in [2, \overline{\alpha}]$ is introduced, as follows:

$$H_{[2,\overline{\alpha}]}(\alpha) = H(2) + H_\alpha(2)(\alpha - 2) + \frac{1}{2!}\overline{H}_{[2,\overline{\alpha}]}(\alpha - 2)^2, \tag{21}$$

where

$$H_{\alpha\alpha}(\theta) \leq \max_{\alpha\in[2,\overline{\alpha}]} H_{\alpha\alpha}(\theta)$$

$$\leq \left(f, \frac{x^2}{1+2x}\right)_+ + \left(f, \frac{x^2}{1+\overline{\alpha}x}\right)_- \equiv \overline{H}_{[2,\overline{\alpha}]}. \tag{22}$$

Finally, α is computed as a solution of the quadratic equation $H_{[\underline{\alpha},2]}(\alpha) = H[f]$ or $H_{[2,\overline{\alpha}]}(\alpha) = H[f]$.

For clarity, the obtained results based on Equations (19)–(22) are compiled in the form of a proposition.

Proposition 1. *The inequality (8), that is,*

$$H[f + \alpha(f^{eq} - f)] \leq H[f]$$

has the following solution.

1. If α^* defined by (17) is smaller than 2, then $\alpha = \min(\underline{\alpha}, \alpha^*)$, where $\underline{\alpha}$ is given by (16).

2. $H[f] = H(0) \leq H(2)$. If $\alpha^* > 2$, then

$$\alpha = 2 + \frac{1}{\overline{H}_{[\underline{\alpha},2]}}\{-H_\alpha(2) + \sqrt{\mathcal{D}}\},$$

where

$$\mathcal{D} = H_\alpha(2)^2 - 2\overline{H}_{[\underline{\alpha},2]}(H(2) - H(0)),$$

moreover, if $\mathcal{D} < 0$, then $\alpha = \underline{\alpha}$.

3. $H[f] = H(0) > H(2)$. If $\overline{\alpha} \geq \alpha^* > 2$, where $\overline{\alpha}$ is given by (18), then $\alpha = 2$. In the case $\alpha^* > \overline{\alpha} \geq 2$ one has

$$\alpha = 2 + \frac{1}{\overline{H}_{[2,\overline{\alpha}]}}\{-H_\alpha(2) + \sqrt{\mathcal{D}}\},$$

where

$$\mathcal{D} = H_\alpha(2)^2 - 2\overline{H}_{[2,\overline{\alpha}]}(H(2) - H(0))$$

and $\overline{H}_{[\underline{\alpha},2]}, \overline{H}_{[2,\overline{\alpha}]}$ are defined by (20) and (22). In addition,

$$H_\alpha(2) = (f, x\log(1+2x)) - (f, x\log(1+x)),$$

$$H_{\alpha\alpha}(2) = \left(f, \frac{x^2}{1+2x}\right).$$

4. Numerical Experiments

In the present paragraph, the numerical solutions of several test problems are considered: the Sod shock tube, the propagation of shear waves and acoustic waves for different angles between a flow direction vector and a perturbation wave-vector, and the double

shear layer. The results are obtained with use of the following entropic LB methods: essentially entropic (EELB) of the first order (used only for Sod shock tube) and the third order [31], the method of Zhao and Yong (ZY) [32], the lower bound $\underline{\alpha}$ evaluated from (16) (used only for the Sod shock tube), and the method described in Proposition 1, defined hereafter as the low-dissipative (LD). During the simulations, the following variables are recorded: the mean, minimal value of α measured over the modeled spatial domain at some moment of time t

$$\langle \alpha \rangle = \frac{1}{n} \sum_{\boldsymbol{x}} \alpha(\boldsymbol{x}), \quad \alpha_{min} = \min_{\boldsymbol{x}} \alpha(\boldsymbol{x}), \tag{23}$$

and L_1, L_2 deviations of α from 2 in the form

$$D_1(\alpha) = \frac{1}{n} \sum_{\boldsymbol{x}} |\alpha(\boldsymbol{x}) - 2|, \tag{24}$$

$$D_2(\alpha) = \sqrt{\frac{1}{n} \sum_{\boldsymbol{x}} (\alpha(\boldsymbol{x}) - 2)^2}, \tag{25}$$

where $\boldsymbol{x}$ denotes spatial nodes, n is the number of the spatial nodes, and, for all modeled problems, $\Delta t = 1$ is used. For convenience, the list of main notations is also given in Appendix A, Table A1.

4.1. Shock Tube

The first test problem is the athermal one-dimensional Sod shock tube. The initial condition is a step density profile: $\rho = 1.5, x \leq H/2, \rho = 0.5, x > H/2$ (i.e., the initial density ratio is 3:1), and H is the length of the domain. For this problem, a grid consisting of 500 spatial nodes is used, and the viscosity is $\nu = 10^{-5}$. Since the problem is one-dimensional, the $D1Q3$ LB model is applied. The equilibrium is taken in the form (3)–(4).

The simulation results for the different entropic LB methods are presented in Figure 3 at the time step $t = 250$. As expected, the density profiles show oscillations [73], and the amplitudes of the oscillations are larger for the less dissipative methods. The first-order EELB method leads to the smallest average values of α (and potentially to the largest dissipation), followed by the method based on $\underline{\alpha}$ from (16), and the method of Zhao and Yong. LD and the third-order EELB are the least dissipative. Moreover, the LD method has the closest to 2 average value of α, that is, it produces the smallest amount of additional dissipation compared to the other methods, but has the largest variations of D_1, D_2, since relatively large values of $\alpha > 2$ are observed (Table 1). Remember that the condition $\alpha > 2$ means that the viscosity is decreased. Note that the dispersive oscillations, which are typical for the ELB method, can be removed by applying LB models with additional artificial viscosity and dispersion terms [74]. In addition, it would be interesting to compare the accuracy of the LB schemes with Navier–Stokes numerical solvers without artificial viscosity [75].

Note that the methods in which α cannot exceed 2 tend to have smaller values of D_1, D_2. Then, in order to test the models under the same conditions, the following experiment has been performed: for the third-order EELB and the present LD method, the variable α has been bounded by 2 in the simulations. In this case, these models show significantly smaller values of D_1, D_2 variances (Table 1). The methods based on $\underline{\alpha}$ from (16) and the first-order EELB give the least accurate solutions to the entropy balance equations and serve as predictors for the LD and third-order EELB methods. In subsequent problems, only the latter approaches are addressed.

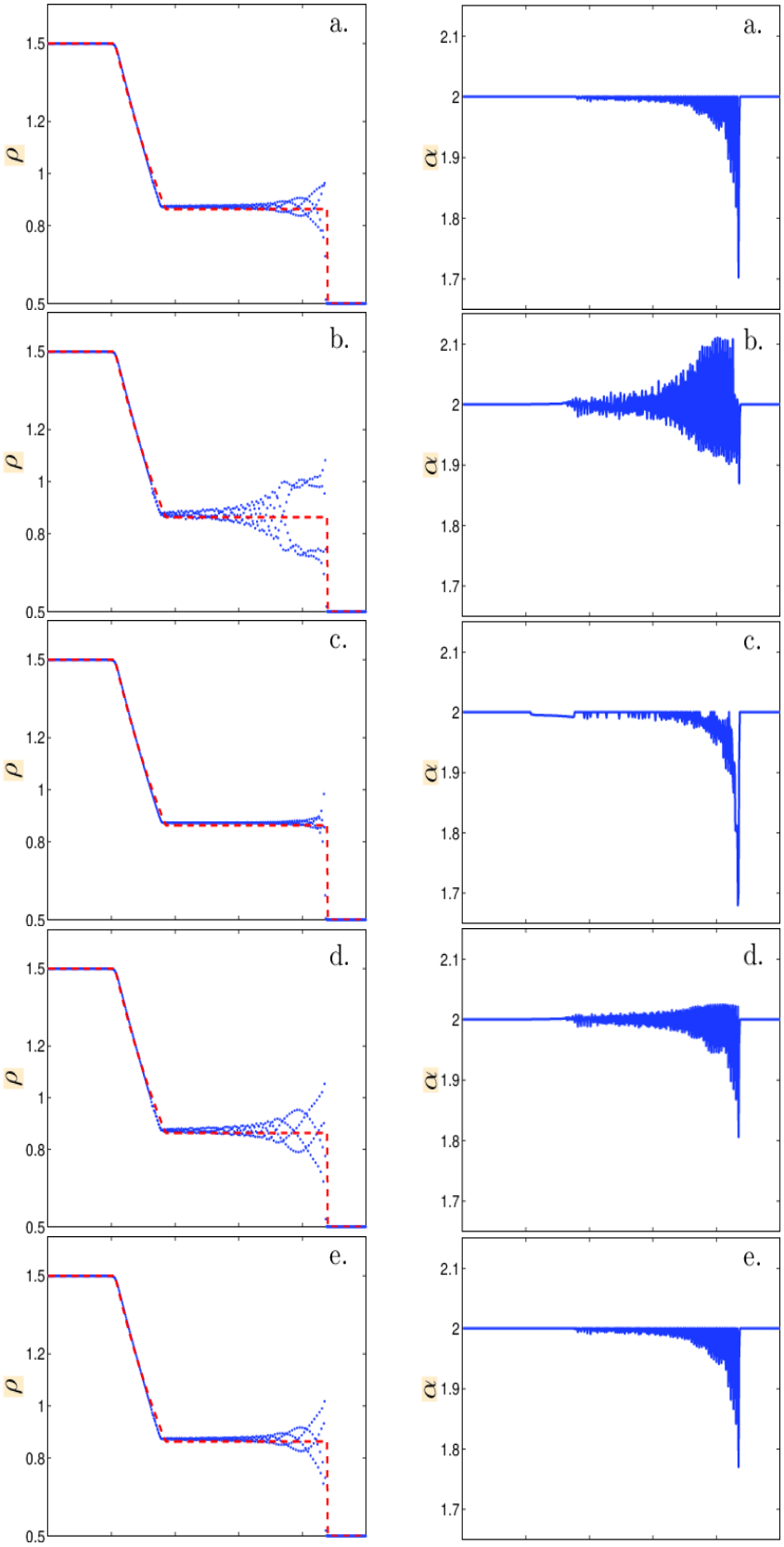

Figure 3. Sod shock tube. The density profiles (**left**) and α (**right**) are presented. From upper to lower slides: (**a**) $\underline{\alpha}$ defined by (16); (**b**) LD method (Proposition 1); (**c**) first-order EELB method; (**d**) third-order EELB method; (**e**) Zhao–Yong method; dashed (red) line is the analytical solution.

Table 1. Sod shock tube. The parameters $\alpha_{min}, \langle\alpha\rangle, D_1, D_2$ defined by (23)–(25) are presented; $\underline{\alpha}$ denotes the method based on Equation (16); LD is the low-dissipative entropic method described in the Proposition 1; EELB 1 is the first-order EELB method; EELB 3 is the third-order EELB method; ZY is the method of Zhao and Yong; LD, $\max(\alpha) = 2$ EELB 3, $\max(\alpha)$ are the low-dissipative entropic and the third-order EELB methods for which α is bounded by 2.

Method	α_{min}	$\langle\alpha\rangle$	D_1	D_2
$\underline{\alpha}$	1.70	1.9956	0.0044	0.020
LD	1.87	1.9997	0.0143	0.029
EELB 1	1.68	1.9916	0.008	0.031
EELB 3	1.81	1.9979	0.008	0.018
ZY	1.77	1.9953	0.005	0.018
LD, $\max(\alpha) = 2$	1.88	1.9962	0.0038	0.0131
EELB 3, $\max(\alpha) = 2$	1.81	1.9963	0.0037	0.0147

4.2. Shear Waves

The simulation of shear waves serves as an excellent test for the assessment of the dissipative properties of the LB models and validation of the linear stability analysis predictions [58]. For this problem, a periodic two-dimensional spatial domain is considered, the initial conditions for the hydrodynamic fields are as follows:

$$\rho|_{t=0} = 1, \tag{26}$$

$$u_x|_{t=0} = c_s Ma - c_s Ma\varepsilon \sin(\varphi(\boldsymbol{k}))\cos(k_x x + k_y y), \tag{27}$$

$$u_y|_{t=0} = \varepsilon c_s Ma \cos(\varphi(\boldsymbol{k}))\cos(k_x x + k_y y), \tag{28}$$

where $\varepsilon = 10^{-4}$, $Ma = 0.2, 0.4$ is the flow Mach number, $\nu = 10^{-5}$, $\boldsymbol{k} = (k_x, k_y)$ is the perturbation wave-number, and $\varphi(\boldsymbol{k}) = \arctan(k_y/k_x)$. In addition, the following variable is introduced: $u_{0,y} = \varepsilon c_s Ma \cos(\varphi(\boldsymbol{k}))$. It would be convenient to introduce the time variable in the form $Fo = k^2\nu t$ (the Fourier number).

The first considered case for the problem (26)–(28) is as follows: $\varphi = 0$ and $k_y = 0$, u_x is constant, and u_y depends only on x. The size of the spatial domain is 32×2 for this case. In addition, $k_x = 2\pi/8$, this means that the perturbation wavelength equals 8 spacings between lattice nodes. The Navier–Stokes equations have the following solution for the velocity u_y:

$$u_y = u_{0,y} \exp(-\nu k_x^2 t).$$

The simulation results are shown in Figure 4 for $Ma = 0.2$ and $Ma = 0.4$ (left slides).

The second case is $k_x = 2\pi/16, k_y = 2\pi/12$. The simulation spatial domain contains 48×36 nodes. Interestingly, this problem is unstable for the third-order recursively regularized LB model [58]. In the present study, all the entropic models are stable but have different dissipation properties. The results are depicted in Figure 4 (right slides).

The ratios ν_e/ν (termed effective viscosity, where ν_e is the viscosity measured during the numerical simulations, and ν is the theoretical viscosity) are shown in Table 2 for both considered cases. Clearly, from the results in Figure 4 and Table 2 one can see that the present LD method has the smallest dissipation among all considered entropic approaches and gives the values of ν_e/ν closest to the ones for the conventional $D2Q9$ model ($\alpha = 2$). It is important to mention that for the $D2Q9$ model, the viscosity decreases if the flow velocity is increased [76]. Such a behavior is stipulated by the cubic defects ($\nabla \cdot (\rho\boldsymbol{uuu})$), which enter the Navier–Stokes equations derived from low-order LB models like $D2Q9$ [70,76,77]. This effect is seen in Tables 2 and 3. The magnitude of the effective viscosity tends to be smaller than unity for the $D2Q9, \alpha = 2$ model.

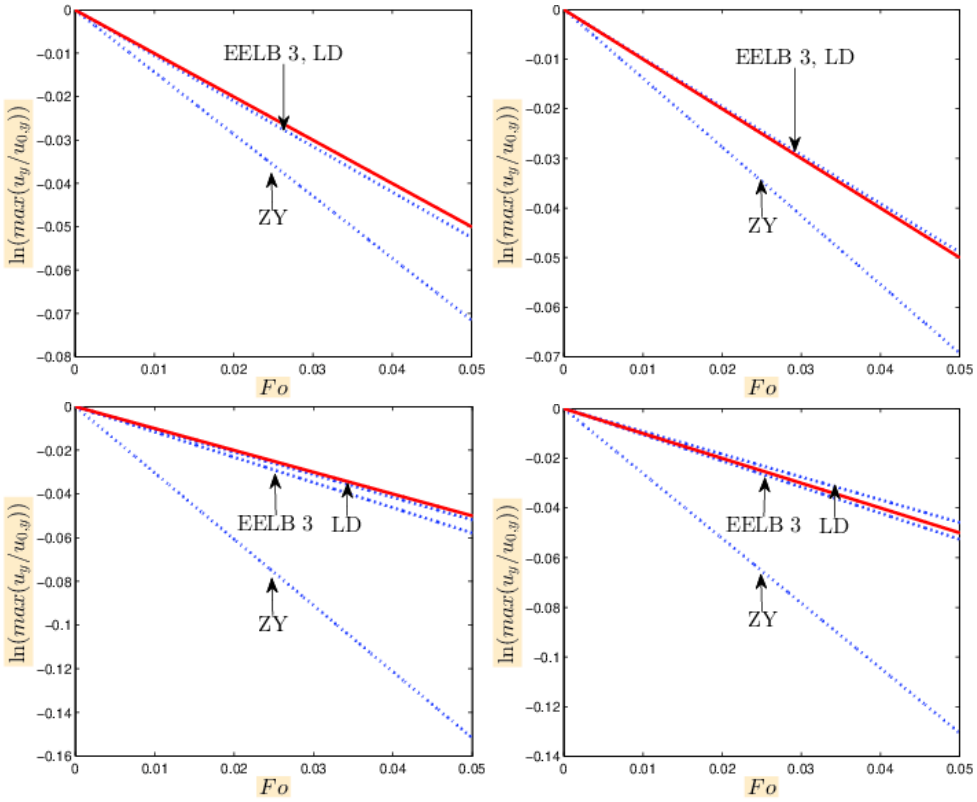

Figure 4. Shear waves, upper slides: $Ma = 0.2$, lower slides: $Ma = 0.4$; left slides: $k_x = 2\pi/8, k_y = 0$; and the right slides: $k_x = 2\pi/16, k_y = 2\pi/12$. LD is the low-dissipative entropic method described in Proposition 1; EELB 3 is the third-order EELB method; ZY is the method of Zhao and Yong. The Navier–Stokes solutions are denoted as: $(-)$.

Table 2. Shear waves, the ratios ν_e/ν (ν_e is the viscosity measured during the numerical simulations, ν is the theoretical viscosity) are presented. $\alpha = 2$ is the standard LB method; LD is the low-dissipative entropic method described in Proposition 1; EELB 3 is the third-order EELB method; ZY is the method of Zhao and Yong.

	$Ma = 0.2$		$Ma = 0.4$	
Model	$k = (\frac{2\pi}{8}, 0)$	$k = (\frac{2\pi}{16}, \frac{2\pi}{12})$	$k = (\frac{2\pi}{8}, 0)$	$k = (\frac{2\pi}{16}, \frac{2\pi}{12})$
$\alpha = 2$	1.05	0.98	1.03	0.91
LD	1.05	0.98	1.04	0.92
$EELB3$	1.05	0.98	1.16	1.05
ZY	1.43	1.39	3.03	2.61

Table 3. Acoustic waves, the ratios ν_e/ν (ν_e is the viscosity measured during the numerical simulations, ν is the theoretical viscosity) are presented. $\alpha = 2$ is the standard LB method; LD is the low-dissipative entropic method described in Proposition 1; EELB 3 is the third-order EELB method; ZY is the method of Zhao and Yong.

	$Ma = 0.2$		$Ma = 0.4$	
Model	$k = (\frac{2\pi}{8}, 0)$	$k = (\frac{2\pi}{16}, \frac{2\pi}{12})$	$k = (\frac{2\pi}{8}, 0)$	$k = (\frac{2\pi}{16}, \frac{2\pi}{12})$
$\alpha = 2$	0.98	1.05	0.86	1.03
LD	0.98	1.05	0.87	1.03
$EELB3$	0.98	1.05	1.01	1.12
ZY	1.41	1.69	4.19	2.53

4.3. Acoustic Waves

This problem involves the variations of density. The initial conditions are given by the following expressions [58]:

$$\rho|_{t=0} = 1 + \delta\rho_0 = 1 + \epsilon\cos(k_x x + k_y y), \tag{29}$$

$$u_x|_{t=0} = c_s Ma + c_s\delta\rho_0\cos(\varphi(\boldsymbol{k})), \tag{30}$$

$$u_y|_{t=0} = c_s\delta\rho_0\sin(\varphi(\boldsymbol{k})), \tag{31}$$

In the simulations, the following values of the parameters are adopted: $\varepsilon = 10^{-4}$, $Ma = 0.2, 0.4$, $\nu = 10^{-5}$, $\varphi(\boldsymbol{k}) = \arctan(k_y/k_x)$.

Similarly to the previous case, the problem (29)–(31) is solved for two combinations of k_x, k_y. The spatial domain is considered as periodic, and the size of the domain is taken as 48×36. Initially, the case $\varphi = 0$ and $k_x = 2\pi/8, k_y = 0$ is considered. The results are plotted in Figure 5 (left slides). Next, the results of the simulations for the inclined acoustic waves $k_x = 2\pi/16, k_y = 2\pi/12$ are presented in Figure 5 (right slides). Again, the application of the LD method only slightly varies the dissipation properties compared to the standard LB model results (Table 3).

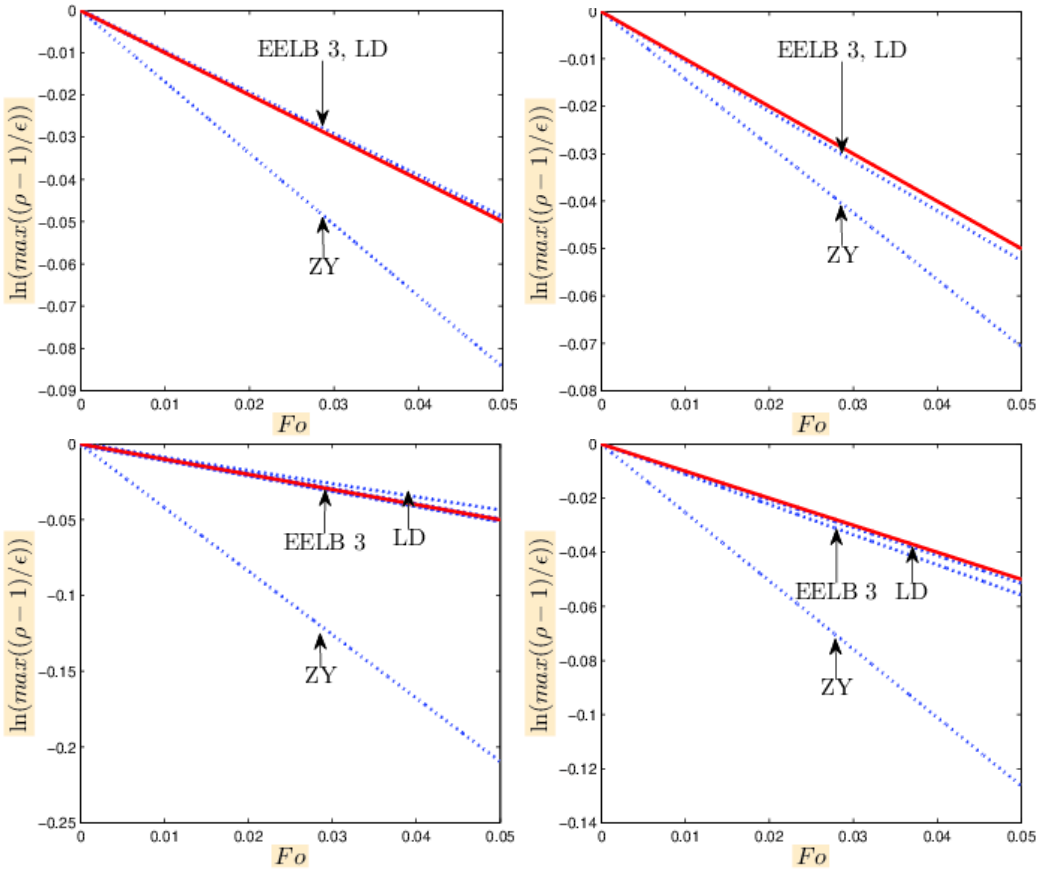

Figure 5. Acoustic waves, upper slides: $Ma = 0.2$, lower slides: $Ma = 0.4$; left slides: $k_x = 2\pi/8, k_y = 0$ and the right slides: $k_x = 2\pi/16, k_y = 2\pi/12$. LD is the low-dissipative entropic method described in Proposition 1; EELB 3 is the third-order EELB method; ZY is the method of Zhao and Yong. The Navier–Stokes solutions are denoted as: $(-)$.

In conclusion, one can notice that the considered entropic methods are significantly better suited for the modeling of shear and acoustic waves than the regularized LB models [58,60] due to the relatively small deviations of the measured efficient viscosities from the theoretical values.

4.4. Double Shear Layer

In this problem, a flow in a doubly periodic two-dimensional square domain of a size $L \times L$ is considered. The initial conditions for the flow velocities are defined as follows:

$$u_x(x,y)|_{t=0} = U_0 \tanh(k(y/L - 0.25)), \quad y < L/2, \tag{32}$$

$$u_x(x,y)|_{t=0} = U_0 \tanh(k(0.75 - y/L)), \quad y \geq L/2, \tag{33}$$

$$u_y(x,y)|_{t=0} = U_0 \delta \sin(2\pi(x/L + 0.25)), \tag{34}$$

where the parameters k, δ are as follows:

$$k = 80, \quad \delta = 0.05$$

The initial density equals 1, and the Reynolds number is $Re = U_0 L/\nu$, where ν is the viscosity.

Note that the form of the initial distribution function noticeably affects the dissipation properties of the flow, so in order to avoid initial spurious oscillations, the distribution function at $t = 0$ is initialized in the regularized form $\boldsymbol{f}^{(eq)} + \boldsymbol{f}^{(1)}$, where the elements of the stress tensor entering the non-equilibrium component of the distribution function $\boldsymbol{f}^{(1)}$ are computed by applying finite-difference approximations [41] of $\boldsymbol{\nabla u}$.

The numerical simulations of the problem (32)–(34) are performed for $Re = 3 \times 10^4$ and $U_0 = 0.04$. This means that the Mach number equals $Ma = U_0/c_s = \sqrt{3} \times 0.04 \approx 0.0693$. It is convenient to introduce the characteristic time variable (convection time) as $t_c = L/U_0$. The flow is assumed to be stable if the solutions remain finite in the time interval $t \in [0, 2t_c]$.

The sensitivity of the entropic methods to the grid resolution can be tested for the present problem. For coarse meshes 64×64 and 128×128, the third-order EELB, Zhao-Yong, and LD methods show qualitatively correct results but produce spurious vortices. These vortices may lead to blow-up instabilities, but in the present case, the solutions are finite because the fulfillment of the entropy balance equation suppresses unstable oscillations. Note that the standard $D2Q9$ model ($\alpha = 2$) is unstable for grid resolutions of 64×64 and 128×128. For grid resolutions larger than 128×128, spurious vortices are not observed, and all approaches produce accurate vortical profiles. In the case of the spatial resolution 256×256, the normalized vorticity profiles are presented for the all considered methods at $t = t_c$ in Figure 6. One can observe that all approaches give very similar results. Next, the time histories of the variables of $\langle\alpha\rangle - 2$ and D_1 are presented in Figure 7. Clearly, the LD method gives the smallest average values of $|\alpha - 2|$ among the all considered methods. In addition, the LD method shows smaller D_1 variances than the third-order EELB method.

Finally, the evolution of the following variables is considered: the averaged on the spatial variables kinetic energy $\langle u^2 \rangle = \langle u_x^2 + u_y^2 \rangle$ normalized on U_0^2 and the averaged on the spatial variables squared vorticity $\langle \omega^2 \rangle$ (enstrophy) normalized on $(U_0/L)^2$. As a benchmark, the simulation results based on the standard $D2Q9$ LB model for a grid with the resolution 1024×1024 are taken (these simulations are stable). From Figure 8, one can observe that all entropic methods show similar results: they are close to the benchmark solution but more dissipative to some extent than the benchmark solution, which uses well-resolved grid. In addition, the LD method is slightly less dissipative than the other entropic treatments.

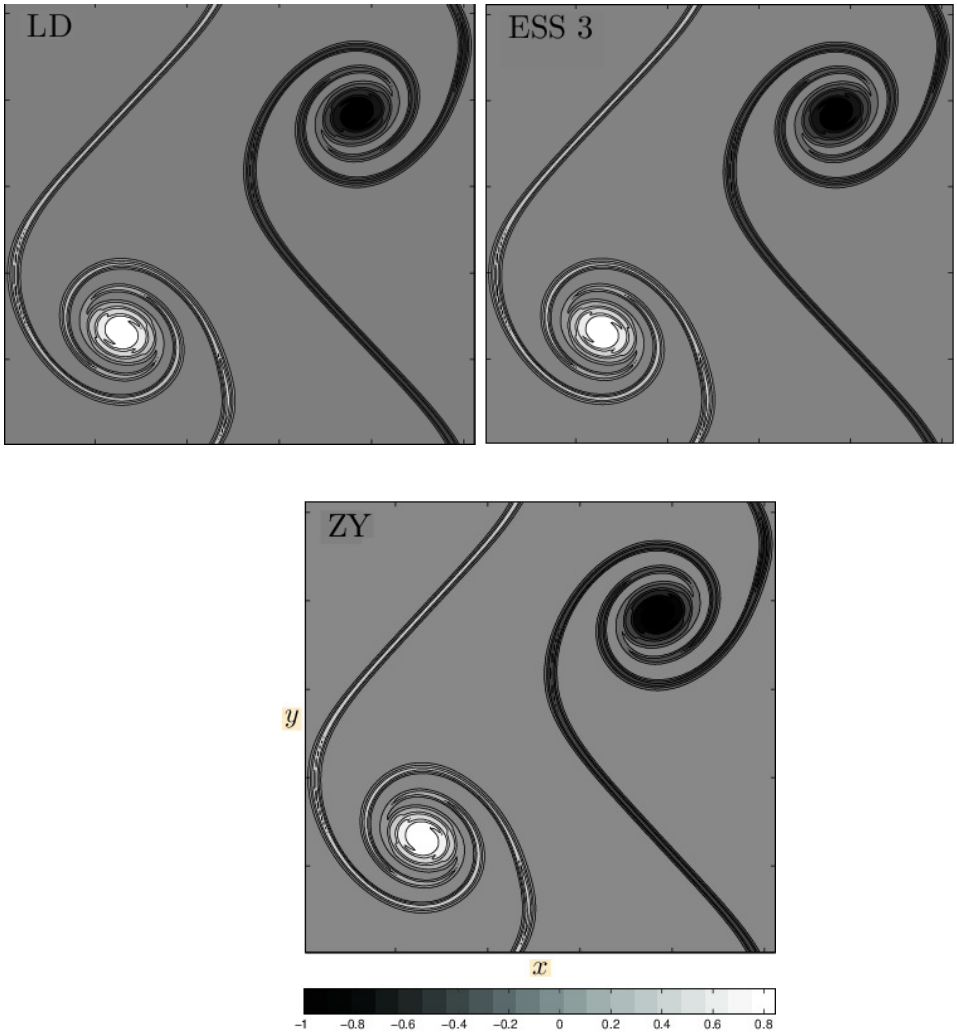

Figure 6. Double shear layer. The grid resolution is 256×256, $Ma = 0.0693, Re = 3 \times 10^4$. The normalized vorticity plots are presented at the moment of time $t = t_c$; LD is the low-dissipative entropic method described in Proposition 1; EELB 3 is the third-order EELB method; ZY is the method of Zhao and Yong.

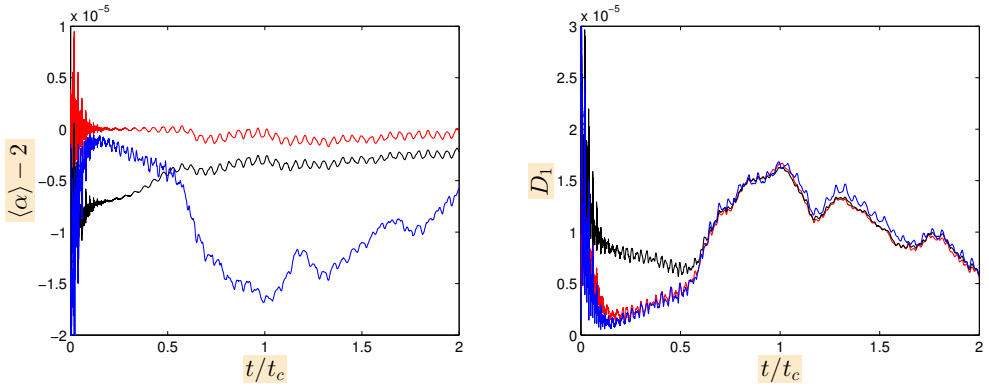

Figure 7. Double shear layer. The grid resolution is 256×256, $Ma = 0.0693, Re = 3 \times 10^4$. The time histories of the variables $\langle \alpha \rangle - 2$ and D_1 are presented; the low-dissipative entropic method is denoted by a red line $(-)$; the third-order EELB method is denoted by a black line $(-)$; the method of Zhao and Yong is denoted by a blue line $(-)$.

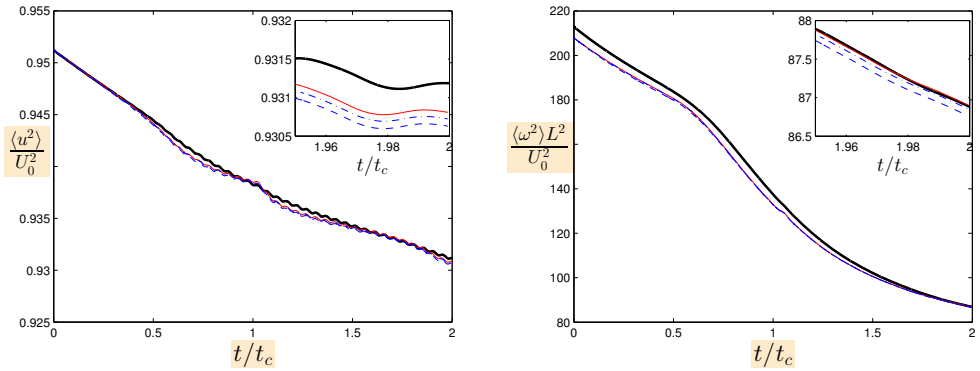

Figure 8. Double shear layer, $Ma = 0.0693, Re = 3 \times 10^4$. The kinetic energy (upper plot) and squared vorticity (lower plot) are presented. The benchmark solution is denoted as $(-)$; the low-dissipative entropic method is denoted as $(-)$; the third-order EELB method is denoted as $(--)$; the method of Zhao and Yong is denoted as $(-\cdot-)$. For all entropic models, the grid resolution is 256×256.

4.5. Performance

The performance of the considered entropic stabilization approaches is affected by the implementation details and the modeled problems. For instance, the method of Zhao and Yong is applied only for the nodes in which the H-theorem is violated. Therefore, this method can be faster than the others if the proportion of the spatial nodes prone to instabilities is small. On the other hand, the Zhao and Yong and the present low-dissipative methods exploit the values of the H-function, which require the computation of logarithms; the latter is relatively slow operation. On average, the LB $D2Q9$ model stabilized by the considered entropic techniques is approximately two to three times slower than the LB $D2Q9$ model without additional stabilization. For example, for the shear waves, the Zhao and Yong method is 2.2 times slower than the conventional $D2Q9$ model followed by the low-disspative and essentially entropic methods, which are 2.38, 2.77 times slower than the conventional $D2Q9$ model. For acoustic waves, the methods of Zhao-Yong, low-dissipative, and essentially entropic are 1.81, 2.0, and 2.38 times slower than the conventional $D2Q9$ model. Note that, in the present study, the simulations are performed with use of self-standing C++ code (and the figures are generated with use of MATLAB). In order to increase the speed of code execution, the dynamic arrays, such as vector class from the standard C++ library, are avoided in the parts of the code related to the entropic stabilizers.

5. Conclusions

In the present study, a novel approach for finding the solutions to the entropy balance Equation (2) is proposed: by employing the bounds for the logarithms, the H-function is approximated by quadratic function on the variable α around $\alpha = 2$; then, the solution for α is obtained analytically from the quadratic algebraic equation. The proposed stabilization technique (termed as low-dissipative) is very "mild" (i.e., the departure of α from its normal value 2 is small). Therefore, the injection of the additional dissipation in the modeled systems is very moderate.

In order to validate the developed method, the following test problems have been considered: the shock tube problem, the propagation of shear waves, acoustic waves, and doubly shear layer problem. In addition, for comparison purposes, these problems have been also solved employing the approaches in which α is given in the form of a closed analytical expression: the essentially entropic LB method [31] and the method of Zhao and Yong [32]. For all problems, the presented method gives the solutions for α that are closest to its normal value 2. For the Sod shock tube problem, one can notice that all entropic methods lead to dispersive oscillations near shock. This behavior is typical for

these models [73]. The entropic methods for which alpha is close to 2 (such as essentially entropic and the present approach) show larger oscillations than more dissipative methods. In addition, it has been shown that, compared to the regularized LB models, the present entropic method is able to reproduce correct attenuation rates for shear and acoustic waves for relatively coarse grids (8–16 nodes per wavelength).

Funding: This work is supported by the Ministry of Science and Higher Education of the Russian Federation, Project No. 075-15-2020-799.

Data Availability Statement: The simulation code that supports the findings of this study is available from the author upon reasonable request.

Conflicts of Interest: The author declares no conflict of interest.

Abbreviations

The following abbreviations are used in this manuscript:

ELB	Entropic lattice Boltzmann
EELB	Essentially entropic lattice Boltzmann
LB	Lattice Boltzmann
LD	Low dissipative
ZY	Zhao Yong

Appendix A

For the sake of clarity, a table containing the main used notations and their corresponding explanations is presented.

Table A1. List of main notations.

Notation	Formula	Explanation
$\underline{\alpha}$	$\frac{(\boldsymbol{f},\boldsymbol{x}\log(1+\boldsymbol{x}))}{\left(\frac{1}{2}(\boldsymbol{f},\boldsymbol{x}^2)-\frac{1}{3}(\boldsymbol{f},\boldsymbol{x}^3)_-+\frac{4}{3}(\boldsymbol{f},\boldsymbol{x}^4)_-\right)}$	lower bound for α
$\overline{\alpha}$	$\frac{2(\boldsymbol{f},\boldsymbol{x}\log(1+\boldsymbol{x}))}{(\boldsymbol{f},\boldsymbol{x}^2)_-}$	upper bound for α
α^*	$\min_{i:f_i-f_i^{eq}>0}\frac{f_i}{f_i-f_i^{eq}}$	upper bound for α
$\langle\alpha\rangle$	$\frac{1}{n}\sum_{\boldsymbol{x}}\alpha(\boldsymbol{x})$	average value of α over spatial domain
α_{min}	$\min_{\boldsymbol{x}}\alpha(\boldsymbol{x})$	minimal value of α in spatial domain
$D_1(\alpha)$	$\frac{1}{n}\sum_{\boldsymbol{x}}\lvert\alpha(\boldsymbol{x})-2\rvert$	L_1 deviations of α from 2 in the spatial domain
$D_2(\alpha)$	$\sqrt{\frac{1}{n}\sum_{\boldsymbol{x}}(\alpha(\boldsymbol{x})-2)^2}$	L_2 deviations of α from 2 in the spatial domain

References

1. Qian, Y.H.; d'Humières, D.; Lallemand, P. Lattice BGK Models for Navier Stokes Equation. *Europhys. Lett.* **1992**, *17*, 479–484. [CrossRef]
2. Guo, Z.; Shu, C. *Lattice Boltzmann Method and Its Applications in Engineering*; World Scientific Publishing Company: Singapore, 2013.
3. Krüger, T.; Kusumaatmaja, H.; Kuzmin, A.; Shardt, O.; Silva, G.; Viggen, E. *The Lattice Boltzmann Method. Principles and Practice*; Springer: Berlin/Heidelberg, Germany, 2017.
4. Succi, S. *The Lattice Boltzmann Equation: For Complex States of Flowing Matter*; Oxford University Press: Oxford, UK, 2018.
5. Jourabian, M.; Darzi, A.A.R.; Toghraie, D.; ali Akbari, O. Melting process in porous media around two hot cylinders: Numerical study using the lattice Boltzmann method. *Phys. A Stat. Mech. Its Appl.* **2018**, *509*, 316. [CrossRef]
6. Zhu, L.; Zhang, H.; Xiao, L.; Bazylak, A.; Gao, X.; Sui, P.C. Pore-scale modeling of gas diffusion layers: Effects of compression on transport properties. *J. Power Sources* **2021**, *496*, 229822. [CrossRef]
7. Suga, K. Lattice Boltzmann methods for complex micro-flows: Applicability and limitations for practical applications. *Fluid Dyn. Res.* **2013**, *45*, 034501. [CrossRef]
8. Mazloomi, A.; Chikatamarla, S.S.; Karlin, I. Entropic Lattice Boltzmann Method for Multiphase Flows. *Phys. Rev. Lett.* **2015**, *114*, 174502. [CrossRef]
9. Nemati, M.; Shateri Najaf Abady, A.R.; Toghraie, D.; Karimipour, A. Numerical investigation of the pseudopotential lattice Boltzmann modeling of liquid-vapor for multi-phase flows. *Phys. A Stat. Mech. Its Appl.* **2018**, *489*, 65. [CrossRef]

10. Toghaniyan, A.; Zarringhalam, M.; Akbari, O.A.; Sheikh Shabani, G.A.; Toghraie, D. Application of lattice Boltzmann method and spinodal decomposition phenomenon for simulating two-phase thermal flows. *Phys. A Stat. Mech. Its Appl.* **2018**, *509*, 673–689. [CrossRef]
11. Ahmadi Balootaki, A.; Karimipour, A.; Toghraie, D. Nano scale lattice Boltzmann method to simulate the mixed convection heat transfer of air in a lid-driven cavity with an endothermic obstacle inside. *Phys. A Stat. Mech. Its Appl.* **2018**, *508*, 681–701. [CrossRef]
12. Dellar, P. Bulk and shear viscosities in lattice Boltzmann equations. *Phys. Rev. E* **2001**, *64*, 031203. [CrossRef]
13. Lallemand, P.; Luo, L.S. Theory of the lattice Boltzmann method: Dispersion, dissipation, isotropy, Galilean invariance, and stability. *Phys. Rev. E* **2000**, *61*, 6546. [CrossRef]
14. d'Humières, D.; Ginzburg, I.; Krafczyk, M.; Lallemand, P.; Luo, L.S. Multiple–relaxation–time lattice Boltzmann models in three dimensions. *Phil. Trans. R. Soc. Lond.* **2002**, *360*, 437. [CrossRef]
15. Lallemand, P.; Luo, L.S. Theory of the lattice Boltzmann method: Acoustic and thermal properties in two and three dimensions. *Phys. Rev. E* **2003**, *68*, 036706. [CrossRef]
16. Ricot, D.; Marié, S.; Sagaut, P.; Bailly, C. Lattice Boltzmann method with selective viscosity filter. *J. Comp. Phys.* **2009**, *228*, 4478. [CrossRef]
17. Li, Y.; Shock, R.; Zhang, R.; Chen, H. Numerical study of flow past an impulsively started cylinder by the lattice-Boltzmann method. *J. Fluid Mech.* **2004**, *519*, 273–300. [CrossRef]
18. Tosi, F.; Ubertini, S.; Succi, S.; Chen, H.; Karlin, I. Numerical stability of Entropic versus positivity-enforcing Lattice Boltzmann schemes. *Math. Comput. Simul.* **2006**, *72*, 227–231. [CrossRef]
19. Karlin, I.; Succi, S.; Chikatamarla, S. Comment on "Numerics of the lattice Boltzmann method: Effects of collision models on the lattice Boltzmann simulations". *Phys. Rev. E* **2011**, *84*, 068701. [CrossRef]
20. Karlin, I.; Bösch, F.; Chikatamarla, S.; Succi, S. Entropy-Assisted Computing of Low-Dissipative Systems. *Entropy* **2015**, *17*, 8099. [CrossRef]
21. Yong, W.A.; Luo, L.S. Nonexistence of H theorems for the athermal lattice Boltzmann models with polynomial equilibria. *Phys. Rev. E* **2003**, *67*, 051105. [CrossRef]
22. Yong, W.A.; Luo, L.S. Nonexistence of H Theorem for some Lattice Boltzmann models. *J. Stat. Phys.* **2005**, *121*, 91. [CrossRef]
23. Karlin, I.; Succi, S. Equilibria for discrete kinetic equations. *Phys. Rev. E* **1998**, *58*, R4053. [CrossRef]
24. Karlin, I.; Gorban, A.; Succi, S.; Boffi, V. Maximum Entropy Principle for Lattice Kinetic Equations. *Phys. Rev. Lett.* **1998**, *81*, 6–9. [CrossRef]
25. Karlin, I.; Ferrante, A.; Öttinger, H. Perfect entropy functions of the Lattice Boltzmann method. *Europhys. Lett.* **1999**, *47*, 182–188. [CrossRef]
26. Ansumali, S.; Karlin, I.; Öttinger, H. Minimal entropic kinetic models for hydrodynamics. *Europhys. Lett.* **2003**, *63*, 798–804. [CrossRef]
27. Ansumali, S.; Karlin, I. Stabilization of the lattice Boltzmann method by the H theorem: A numerical test. *Phys. Rev E* **2000**, *62*, 7999. [CrossRef] [PubMed]
28. Ansumali, S.; Karlin, I. Entropy Function Approach to the Lattice Boltzmann Method. *J. Stat. Phys.* **2002**, *107*, 291. [CrossRef]
29. Tosi, F.; Ubertini, S.; Succi, S.; Karlin, I. Optimization Strategies for the Entropic Lattice Boltzmann Method. *J. Sci. Comput.* **2007**, *30*, 369–387. [CrossRef]
30. Chikatamarla, S.; Ansumali, S.; Karlin, I. Entropic Lattice Boltzmann Models for Hydrodynamics in Three Dimensions. *Phys. Rev. Lett.* **2006**, *97*, 010201. [CrossRef]
31. Atif, M.; Kolluru, P.; Thantanapally, C.; Ansumali, S. Essentially Entropic Lattice Boltzmann Model. *Phys. Rev. Lett.* **2017**, *119*, 240602. [CrossRef]
32. Zhao, W.; Yong, W.A. Relaxation-rate formula for the entropic lattice Boltzmann method. *Chin. Phys. B* **2019**, *28*, 114701. [CrossRef]
33. Jonnalagadda, A.; Sharma, A.; Agrawal, A. Single Relaxation Time Entropic Lattice Boltzmann Methods: A Developer's Perspective for Stable and Accurate Simulations. *Comput. Fluids* **2021**, *2015*, 104792. [CrossRef]
34. Brownlee, R.; Gorban, A.; Levesley, J. Stabilization of the lattice Boltzmann method using the Ehrenfests' coarse-graining idea. *Phys. Rev. E* **2006**, *74*, 037703. [CrossRef]
35. Brownlee, R.; Gorban, A.; Levesley, J. Nonequilibrium entropy limiters in lattice Boltzmann methods. *Phys. A Stat. Mech. Its Appl.* **2007**, *387*, 385–406. [CrossRef]
36. Gorban, A.; Packwood, D. Enhancement of the stability of lattice Boltzmann methods by dissipation control. *Phys. A Stat. Mech. Its Appl.* **2014**, *414*, 285. [CrossRef]
37. Latt, J.; Coreixas, C.; Beny, J.; Parmigiani, A. Efficient supersonic flow simulations using lattice Boltzmann methods based on numerical equilibria. *Phil. Trans. R. Soc.* **2020**, *378*, 20190559. [CrossRef]
38. Coreixas, C.; Latt, J. Compressible lattice Boltzmann methods with adaptive velocity stencils: An interpolation-free formulation. *Phys. Fluids* **2020**, *32*, 116102. [CrossRef]
39. Karlin, I.; Bösch, F.; Chikatamarla, S. Gibbs' principle for the lattice-kinetic theory of fluid dynamics. *Phys. Rev. E* **2014**, *90*, 031302(R). [CrossRef]

40. Bösch, F.; Chikatamarla, S.; Karlin, I. Entropic Multi-Relaxation Models for Simulation of Fluid Turbulence. *ESAIM Proc. Surv.* **2015**, *52*, 1. [CrossRef]
41. Mattila, K.; Hegele, L., Jr.; Philippi, P. Investigation of an entropic stabilizer for the lattice-Boltzmann method. *Phys. Rev. E* **2015**, *91*, 063010. [CrossRef]
42. Wang, L. Enhanced multi-relaxation-time lattice Boltzmann model by entropic stabilizers. *Phys. Rev. E* **2020**, *102*, 023307. [CrossRef]
43. Latt, J.; Chopard, B. Lattice Boltzmann method with regularized pre-collision functions. *Math. Comput. Simul.* **2006**, *72*, 165. [CrossRef]
44. Chen, H.; Zhang, R.; Staroselsky, I.; Jhon, M. Recovery of full rotational invariance in lattice Boltzmann formulations for high Knudsen number flows. *Phys. A Stat. Mech. Appl.* **2006**, *362*, 125–131. [CrossRef]
45. Latt, J. Hydrodynamic Limit of Lattice Boltzmann Equations. Ph.D. Thesis, University of Geneva, Geneva, Switzerland, 2007.
46. Malaspinas, O. Increasing stability and accuracy of the lattice Boltzmann scheme: Recursivity and regularization. *arXiv* **2015**, arXiv:1505.06900.
47. Brogi, F.; Malaspinas, O.; Chopard, B.; Bonadonna, C. Hermite regularization of the lattice Boltzmann method for open source computational aeroacoustics. *J. Acoust. Soc. Amer.* **2017**, *142*, 2332. [CrossRef] [PubMed]
48. Coreixas, C.; Wissocq, G.; Puigt, G.; Boussuge, J.F.; Sagaut, P. Recursive regularization step for high-order lattice Boltzmann methods. *Phys. Rev. E* **2017**, *96*, 033306. [CrossRef] [PubMed]
49. Mattila, K.; Philippi, P.; Hegele, L., Jr. High-order regularization in lattice-Boltzmann equations. *Phys. Fluids* **2017**, *29*, 046103. [CrossRef]
50. Coreixas, C. High-Order Extension of the Recursive Regularized Lattice Boltzmann Method. Ph.D. Thesis, Institut National Polytechnique de Toulouse, Toulouse, France, 2018.
51. Coreixas, C.; Chopard, B.; Latt, J. Comprehensive comparison of collision models in the lattice Boltzmann framework: Theoretical investigations. *Phys. Rev. E* **2019**, *100*, 033305. [CrossRef]
52. Feng, Y.; Boivin, P.; Jacob, J.; Sagaut, P. Hybrid recursive regularized thermal lattice Boltzmann model for high subsonic compressible flows. *J. Comput. Phys.* **2019**, *394*, 82–99. [CrossRef]
53. Chen, H.; Zhang, R.; Gopalakrishnan, P. Filtered lattice Boltzmann collision formulation enforcing isotropy and Galilean invariance. *Phys. Scr.* **2020**, *95*, 034003. [CrossRef]
54. Jonnalagadda, A.; Sharma, A.; Agrawal, A. Onsager-regularized lattice Boltzmann method: A nonequilibrium thermodynamics-based regularized lattice Boltzmann method. *Phys. Rev. E* **2021**, *104*, 015313. [CrossRef]
55. Jonnalagadda, A.; Sharma, A.; Agrawal, A. Revisiting the Lattice Boltzmann Method Through a Nonequilibrium Thermodynamics Perspective. *J. Heat Transfer.* **2021**, *143*, 052102. [CrossRef]
56. Krämer, A.; Wilde, D.; Küllmer, K.; Reith, D.; Foysi, H. Pseudoentropic derivation of the regularized lattice Boltzmann method. *Phys. Rev. E* **2019**, *100*, 023302. [CrossRef]
57. Coreixas, C.; Wissocq, G.; Chopard, B.; Latt, J. Impact of collision models on the physical properties and the stability of lattice Boltzmann methods. *Phil. Trans. R. Soc. A* **2020**, *378*, 20190397. [CrossRef]
58. Wissocq, G.; Coreixas, C.; Boussuge, J.F. Linear stability and isotropy properties of athermal regularized lattice Boltzmann methods. *Phys. Rev. E* **2020**, *102*, 053305. [CrossRef]
59. Wissocq, G.; Sagaut, P. Hydrodynamic limits and numerical errors of isothermal lattice Boltzmann schemes. *J. Comput. Phys.* **2022**, *450*, 110858. [CrossRef]
60. Ilyin, O. Discrete-velocity Boltzmann model: Regularization and linear stability. *Phys. Rev. E* **2022**, *105*, 045312. [CrossRef]
61. Qian, Y.H. Fractional Propagation and the Elimination of Staggered Invariants in Lattice-BGK Models. *Intern. J. Mod. Phys. C* **1997**, *8*, 753–761. [CrossRef]
62. Guo, Z.; Zheng, C.; Zhao, T.S. A Lattice BGK Scheme with General Propagation. *J. Sci. Comput.* **2001**, *16*, 569–585. [CrossRef]
63. Zhang, R.; Chen, H.; Qian, Y.H.; Chen, S. Effective volumetric lattice Boltzmann scheme. *Phys. Rev. E* **2001**, *63*, 056705. [CrossRef]
64. Fan, H.; Zhang, R.; Chen, H. Extended volumetric scheme for lattice Boltzmann models. *Phys. Rev. E* **2006**, *73*, 066708. [CrossRef]
65. Guo, X.; Shi, B.; Chai, Z. General propagation lattice Boltzmann model for nonlinear advection-diffusion equations. *Phys. Rev. E* **2018**, *97*, 043310. [CrossRef]
66. Zhao, W.; Yong, W.A. Boundary Scheme for a Discrete Kinetic Approximation of the Navier–Stokes Equations. *J. Sci. Comput.* **2020**, *82*, 71. [CrossRef]
67. Zhao, J.; Zhao, W.; Zhang, Z. Second-order boundary schemes for the lattice Boltzmann method with general propagation. *J. Comput. Phys.* **2020**, *419*, 109669. [CrossRef]
68. Ilyin, O. Second order accurate boundary conditions for the general propagation lattice Boltzmann method. *Phys. Fluids* **2021**, *33*, 033110. [CrossRef]
69. Karlin, I.; Ansumali, S.; Frouzakis, C.; Chikatamarla, S. Elements of the lattice Boltzmann method I: Linear advection equation. *Commun. Comput. Phys.* **2006**, *1*, 1–45.
70. Shan, X.; Yuan, X.F.; Chen, H. Kinetic theory representation of hydrodynamics: A way beyond the Navier–Stokes equation. *J. Fluid Mech.* **2006**, *550*, 413–441. [CrossRef]
71. Atif, M.; Kolluru, P.; Ansumali, S. Essentially entropic lattice Boltzmann model: Theory and simulations. *arXiv* **2022**, arXiv:2203.12946v1.

72. Topsøe, F. *Some Bounds for the Logarithmic Function*; University of Copenhagen: Copenhagen, Denmark, 2007. Available online: https://rgmia.org/papers/v7n2/pade.pdf (accessed on 5 September 2022).
73. Packwood, D. Entropy balance and dispersive oscillations in lattice Boltzmann models. *Phys. Rev. E* **2009**, *80*, 067701. [CrossRef]
74. Gan, Y.B.; Xu, A.G.; Zhang, G.C.; Zhang, P.; Li, Y.J. Finite-Difference Lattice Boltzmann Scheme for High-Speed Compressible Flow: Two Dimensional Case. *Commun. Theor. Phys.* **2008**, *50*, 201.
75. Rostamzadeh, A.; Razavi, S.E.; Mirsajedi, S.M. Towards Multidimensional Artificially Characteristic-Based Scheme for Incompressible Thermo-Fluid Problems. *Mechanika* **2017**, *23*, 826–834. [CrossRef]
76. Dellar, P. Lattice Boltzmann algorithms without cubic defects in Galilean invariance on standard lattices. *J. Comput. Phys.* **2014**, *259*, 270–283. [CrossRef]
77. Ilyin, O. Discrete Velocity Boltzmann Model for Quasi-Incompressible Hydrodynamics. *Mathematics* **2021**, *9*, 993. [CrossRef]